Available online at www.sciencedirect.com
SCIENCE DIRECT®
Astroparticle Physics 21 (2004) 583–596
Astroparticle Physics
www.elsevier.com/locate/astropart

The cosmic ray primary composition in the "knee" region through the EAS electromagnetic and muon measurements at EAS-TOP

EAS-TOP Collaboration

M. Aglietta [a,b], B. Alessandro [b,*], P. Antonioli [c], F. Arneodo [d], L. Bergamasco [b,e], M. Bertaina [b,e], C. Castagnoli [e], A. Castellina [a,b], A. Chiavassa [b,e], G. Cini Castagnoli [b,e], B. D'Ettorre Piazzoli [f], G. Di Sciascio [f], W. Fulgione [a,b], P. Galeotti [b,e], P.L. Ghia [a,d], M. Iacovacci [f], G. Mannocchi [a,b], C. Morello [a,b], G. Navarra [b,e], O. Saavedra [b,e], G.C. Trinchero [a,b], S. Valchierotti [b,e], P. Vallania [a,b], S. Vernetto [a,b], C. Vigorito [b,e]

[a] *Istituto di Fisica dello Spazio, Interplanetario, CNR, 10133 Torino, Italy*
[b] *Istituto Nazionale di Fisica Nucleare, 10125 Torino, Italy*
[c] *Istituto Nazionale di Fisica Nucleare, 40126 Bologna, Italy*
[d] *Laboratori Nazionali del Gran Sasso, INFN, 67010 Assergi (AQ), Italy*
[e] *Dipartimento di Fisica Generale dell' Università, 10125 Torino, Italy*
[f] *Dipartimento di Scienze Fisiche dell' Università and INFN, 80125 Napoli, Italy*

Received 17 March 2004; accepted 27 April 2004
Available online 18 May 2004

Abstract

The evolution of the cosmic ray primary composition in the energy range 10^6–10^7 GeV (i.e. the "knee" region) is studied by means of the e.m. and muon data of the Extensive Air Shower EAS-TOP array (Campo Imperatore, National Gran Sasso Laboratories). The measurement is performed through: (a) the correlated muon number (N_μ) and shower size (N_e) spectra, and (b) the evolution of the average muon numbers and their distributions as a function of the shower size. From analysis (a) the dominance of helium primaries at the knee, and therefore the possibility that the knee itself is due to a break in their energy spectrum (at $E_k^{He} = (3.5 \pm 0.3) \times 10^6$ GeV) are deduced. Concerning analysis (b), the measurement accuracies allow the classification in terms of three mass groups: *light* (p,He), *intermediate* (CNO), and *heavy* (Fe). At primary energies $E_0 \approx 10^6$ GeV the results are consistent with the extrapolations of the data from direct experiments. In the knee region the obtained evolution of the energy spectra leads to: (i) an average steep spectrum of the *light* mass group ($\gamma_{p,He} > 3.1$), (ii) a spectrum of the *intermediate* mass group harder than the one of the *light* component ($\gamma_{CNO} \simeq 2.75$, possibly bending at $E_k^{CNO} \approx (6–7) \times 10^6$ GeV), (iii) a constant slope for the spectrum of the

* Corresponding author. Tel.: +39-011-6707370; fax: +39-011-6699579.
E-mail address: alessandro@to.infn.it (B. Alessandro).

0927-6505/$ - see front matter
doi:10.1016/j.astropartphys.2004.04.005

heavy primaries ($\gamma_{Fe} \simeq 2.3$–2.7) consistent with the direct measurements. In the investigated energy range, the average primary mass increases from $\langle \ln A \rangle = 1.6$–$1.9$ at $E_0 \simeq 1.5 \times 10^6$ GeV to $\langle \ln A \rangle = 2.8$–$3.1$ at $E_0 \simeq 1.5 \times 10^7$ GeV. The result supports the standard acceleration and propagation models of galactic cosmic rays that predict rigidity dependent cut-offs for the primary spectra of the different nuclei. The uncertainties connected to the hadronic interaction model (QGSJET in CORSIKA) used for the interpretation are discussed.

PACS: 96.40.De; 96.40.Pq; 26.45.+h
Keywords: Cosmic rays composition; High energies; Extensive Air Showers; Knee

1. Introduction

The bending observed at primary energy $E_0 \approx 3 \times 10^6$ GeV [1,2] represents a main feature of the cosmic ray spectrum. Its understanding can therefore provide a clue for the comprehension of the origin of the galactic cosmic radiation, as it was discussed already in the sixties in terms of propagation [3,4], and more recently in terms of source effects [5,6]. At such energies, the measurements have still to be indirect, i.e. based on the detection of the cascades (Extensive Air Showers, EAS) produced by the primary interactions in the atmosphere, and moreover in an energy region still not fully explored by accelerator measurements. The observation of the changing slope of the electromagnetic (e.m.) EAS size spectrum [1] (henceforward called "knee") was therefore followed by a long debate, whether it should be ascribed to astrophysical phenomena or to an unexpected change in the properties of hadron interactions at such energies. Corresponding features have now been reported in the muon number spectrum [7,8], Cherenkov light [9], and hadronic [10] components. The consistency of such observations, together with the expected absorption in the atmosphere of the shower size value at the break [11], do not support the requirement of sharp changes in the character of the interaction, and therefore the astrophysical interpretation becomes natural. On the other side, the standard galactic acceleration and propagation models predict rigidity dependent breaks in the spectra of the primary nuclei, and therefore the knowledge of the spectra of the different primaries is of main significance for proving such general view. The e.m. and muon data still represent a main tool for the analysis of the knee in terms of spectra and evolution of the primary composition.

We present here the study of the CR primary composition in the knee region ($E_0 = 10^6$–10^7 GeV) based on the data recorded with the Extensive Air Shower EAS-TOP array. The independent e.m. (N_e) and muon (N_μ) size spectra and the $N_e - N_\mu$ combined analysis are presented and discussed. The information on the primary composition is obtained through the analysis of the muon density (average values and whole distributions) vs the shower size (N_e). The interpretation of the experimental measurements has been performed following simulations based on the QGSJET model [12] as implemented in the CORSIKA code [13]. The uncertainties connected to such choice are discussed.

2. The detectors and the data

The EAS-TOP array was located at Campo Imperatore, National Gran Sasso Laboratories, 2005 m a.s.l., 820 g cm^{-2} atmospheric depth (see Fig. 1).

The e.m. detector [11,14] consisted of 35 modules, 10 m^2 each, of plastic scintillators distributed over an area of 10^5 m^2. In the present work, events with at least six nearby modules fired, and the largest number of particles recorded by a module internal to the edges of the array ("internal events") are selected. The core location (X_c, Y_c), the e.m. shower size (N_e) and the slope of the lateral distribution function (s parameter) are obtained fitting the recorded number of particles in each module with the Nishimura–Kamata–Greisen (NKG) expression [15]. The resolutions of such

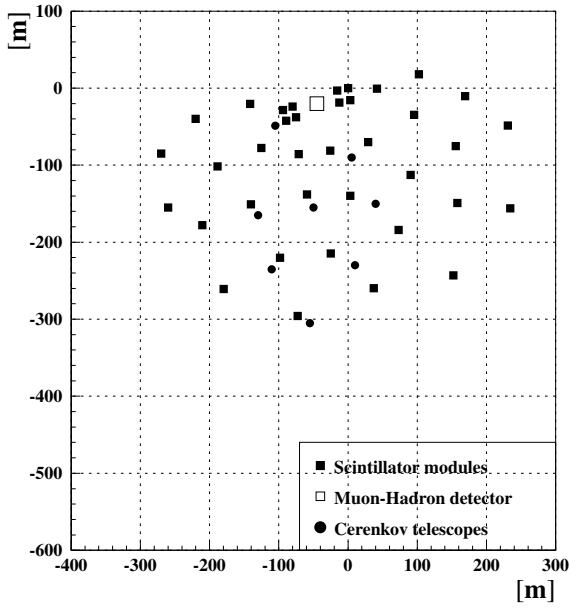

Fig. 1. The EAS-TOP array.

measurements have been obtained by analyzing simulated events in which all experimental uncertainties have been included. Comparing the generated events with the reconstructed ones for sizes $N_e > 2 \times 10^5$ we obtain: $\sigma_{N_e}/N_e \simeq 0.1$; $\sigma_{X_c} = \sigma_{Y_c} \simeq 5$ m; $\sigma_s \simeq 0.1$. The arrival direction of the shower is measured from the times of flight among the modules with resolution $\sigma_\theta \simeq 0.9°$. The triggering condition is fully efficient for $N_e > 10^5$, i.e. for primary energies $E_0 > 3 \times 10^5$ GeV for proton, and $E_0 > 8 \times 10^5$ GeV for iron nuclei.

The muon–hadron detector [16] for the present analysis was used as a tracking module of nine active planes. Each plane included two layers of streamer tubes (12 m length, 3×3 cm^2 section) for muon tracking, one layer of proportional tubes for hadron calorimetry, 8 cm of air and 13 cm of iron shield. The total height of the detector was 280 cm and the surface 12×12 m^2. The tracking tubes operated in limited streamer regime with an argon/isobutane 50/50 gas mixture at a voltage supply of 4650 V. The gas mixture, voltage supply, current and counting rate stability of each layer were continuously monitored. Triggering was provided by the quoted six-fold coincidence of the e.m. array. The charges collected by the anode wires and induced on 3 cm width strips orthogonal to the wires, were extracted and discriminated.

The X, Y and Z coordinates of the crossing particles are provided by the positions of the fired anode wires and strips, and by the level of the layer. The efficiency in the detection of the single hit is $\epsilon_{hit} \simeq 95\%$. A muon track is defined from the alignment of at least 6 fired wires in different streamer tube layers, the energy threshold is $E_\mu^{th} \simeq 1$ GeV. From visual checks, we verified that the reconstruction algorithm does not introduce any error in muon counting up to $N_{track} = 15$ tracks in the module; for larger track numbers an uncertainty is introduced, reaching $\Delta N_{track} = 2$ for $N_{track} = 30$.

The muon analysis is performed by using:

(a) the recorded muon number and density. In particular we use the number of muons $N_{\mu_{180}}$ and the muon density $\rho_{\mu_{180}}$ in events in which the tracking detector distance from the core location (X_c, Y_c) lies between 180 and 210 m; and
(b) the muon size, which is calculated using the same average muon lateral distribution function for data and simulations:

$$N_\mu = \rho_\mu(r) \frac{r_0^{1.25} r^{0.75}}{0.269} \left(1 + \frac{r}{r_0}\right)^{2.5} \quad (1)$$

where $r_0 = 300$ m, r is the distance between the center of muon detector and the core of the shower, $\rho_\mu(r)$ is the recorded muon density. The systematic error (obtained from the simulations) introduced by such procedure in the determination of N_μ does not exceed 6–7% over the whole energy range.

The analysis of the correlated e.m. and muon data presented in the following is performed on a data set collected in 8600 h; runs without snow at the site have been selected. The analysis is presented for events in the shower size interval N_e from $\mathrm{Log}N_e \simeq 5.2$ to 6.6, the observed knee being in a central position. The study of the primary composition is performed for vertical events, i.e. events with zenith angle of the e.m. shower $\theta \leqslant 17.7°$. The number of events used in the

different analysis is given in the tables or captions where the results are reported.

3. The simulations

3.1.

Events have been simulated with the CORSIKA [13] code by using QGSJET [12] as high energy hadronic interaction model, and the analytic treatment of the e.m. component given by the NKG formula [15]. The fluctuations and experimental uncertainties, as well as the trigger requirements, of the e.m. detector have been included by means of parameterized expressions. The full response of the muon detector is included by means of simulations based on the GEANT3 [17] code, and the measured experimental efficiencies of the streamer tubes. The simulated events for both detectors have been treated following the same procedure as the experimental data.

The nuclear elements considered in the simulations are: p, He, N (for CNO), Mg, Fe for a number of events almost equal to the experimental one. The primary energy spectra are simulated with power laws with spectral indexes $\gamma = 2.75$ for protons and $\gamma = 2.65$ for all heavier nuclei. From such data different spectral shapes for different analysis are produced by means of resampling procedures.

The resulting shower size to energy conversion for $\theta < 17.7^\circ$ showers, as a function of the primary mass (A), can be parameterized as in the following:

$$E_0[\mathrm{GeV}] \approx 10^{6.35+0.21\mathrm{Log}A} \cdot (N_e/10^6)^{0.9-0.04\mathrm{Log}A} \qquad (2)$$

3.2.

The capability of QGSJET, as implemented in CORSIKA, of describing the EAS properties has been studied through the EAS-TOP hadrons [18], high energy muons (MACRO) plus Cherenkov light (EAS-TOP) data up to about 10^5 GeV [19], and by the KASCADE group, mainly through the hadrons in EAS in the region around the knee [20]. A proof of its reliability in reproducing the e.m. and muon data is finally provided by the consistency of the conclusions on the primary composition reported by the present work and by the combined EAS-TOP and MACRO measurements (see Section 7). The muon energies recorded in such experiment ($E_\mu > 1.3$ TeV), are indeed related to secondaries produced in a quite different kinematic range with respect to the present ones ($E_\mu > 1$ GeV), i.e. above the central rapidity region [21].

A quantitative comparison, relevant for the present analysis, of the predictions of different hadron interaction models is reported in Fig. 2 where the $N_\mu - N_e$ relationship for proton primaries, is reported for the most qualified and recent models included in CORSIKA (QGSJET [12], NEXUS [22], DPMJET [23], VENUS [24]). The QGSJET predictions result intermediate with respect to the other ones, and the maximum differences in the GeV muon yield for fixed N_e are 15% and 25% respectively below and above the knee. The slopes of the $N_\mu - N_e$ relationship in terms of the exponent α of expression $N_\mu \propto N_e^\alpha$ are: $\alpha = 0.792 \pm 0.007$ for QGSJET, 0.820 ± 0.007

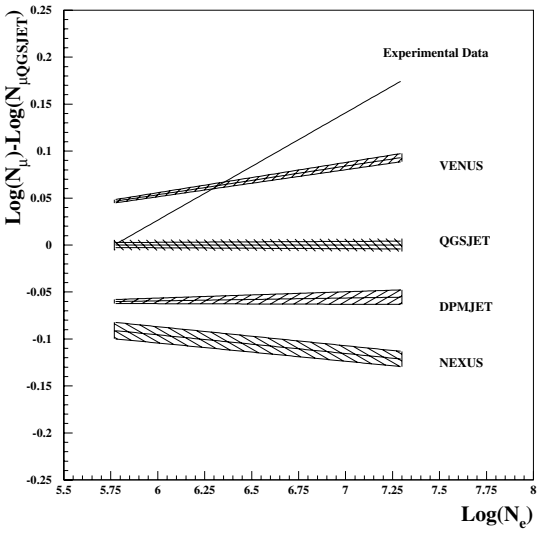

Fig. 2. Comparison between the N_μ–N_e relationships obtained for different interaction models (proton primaries). Data are normalized to QGSJET. The slope of the N_μ–N_e relationship for the experimental data (also plotted) is obtained as explained in Section 5(i); (see for discussion Section 5(iv)).

(VENUS), 0.77 ± 0.02 (NEXUS), 0.789 ± 0.008 (DPMJET). We will therefore consider such differences as the uncertainties related to the choice of a specific interaction model.

4. The electromagnetic and muon size spectra; the dominating component at the knee

4.1.

In a previous paper [11] the analysis of the size spectrum N_e at different zenith singles in the knee region has been presented. First data on the muon size spectrum (calculated as defined in expression (1) for events selected in the range of distances 145 m$< r <$ 170 m between the core and the muon detector) have been presented in [7].

The data around the knee have been fitted with two intersecting power laws both for the e.m. and muon components:

$$\frac{dI}{dN_{e,\mu}} = S_{ke,\mu}\left(\frac{N_{e,\mu}}{N_{ke,\mu}}\right)^{-\gamma^{1,2}_{e,\mu}} \quad (3)$$

where $N_{e,\mu}$ is the e.m. (N_e) or muon size (N_μ), $N_{ke,\mu}$ is the knee position in the e.m. and muon size spectra, $\gamma^{1,2}_{e,\mu}$ are the spectral indexes below ($\gamma^1_{e,\mu}$) and above ($\gamma^2_{e,\mu}$) the knee and $S_{ke,\mu}$ the intensity corresponding to $N_{ke,\mu}$. The χ^2 fit of the experimental data with expression (3) is performed by introducing the instrumental and poissonian fluctuations (particularly relevant for muon data). The results of the analysis of the two size spectra, in different intervals of zenith angles, are reported in Tables 1 and 2. The fits of the N_e spectra are performed for the 8 points symmetric with respect to the knee values reported in paper [11], and, for γ^1_e the weighted mean of the values reported in [11]: $\gamma^1_e = 2.56 \pm 0.02$ has been used (all such values being compatible). The N_e and N_μ spectra are shown in Figs. 3 and 4, together with the results of the fits. The change in slope of the N_μ spectrum is not self evident, since its whole shape is affected by the poissonian fluctuations. To illustrate such feature a second value of χ^2/d.f.(χ^2_1/d.f.) is given for the case of fit performed with a single power law, showing that such solution provides worse results. Also due to the fluctuations, the fit cannot be represented with power law shapes, and therefore the individual points are shown in Fig. 4.

The dispersion of the obtained intensities above the knee ($I(> N_{ek})$ and $I(> N_{\mu k})$) for the two

Table 1
Parameters of the e. m. size spectra (N_e) in different intervals of zenith angles

$\Delta \sec\theta$	γ^1_e	γ^2_e	$I(> N_{ek} \times 10^7)$ $m^{-2}\,s^{-1}\,sr^{-1}$	$\mathrm{Log}(N_{ek})$	χ^2/d.f.
1.00–1.05	2.56	2.96 ± 0.06	1.1 ± 0.1	6.08 ± 0.03	7.8/11
1.05–1.10	2.56	2.86 ± 0.05	1.3 ± 0.2	5.95 ± 0.04	8.4/11
1.10–1.15	2.56	2.86 ± 0.04	1.0 ± 0.1	5.95 ± 0.01	5.3/11
1.15–1.20	2.56	2.82 ± 0.08	0.8 ± 0.2	5.92 ± 0.06	7.6/11
1.27–1.25	2.56	2.92 ± 0.09	0.5 ± 0.1	5.94 ± 0.05	4.6/11
1.25–1.30	2.56	2.75 ± 0.07	1.4 ± 0.4	5.62 ± 0.07	2.8/11

The statistics refers to 10,099 h of data taking, for a total of 2.3×10^7 events.

Table 2
Parameters of the muon size spectra (N_μ) in different intervals of zenith angles

$\Delta \sec\theta$	γ^1_μ	γ^2_μ	$I(> N_{\mu k} \times 10^7)$ $m^{-2}\ s^{-1}\,sr^{-1}$	$\mathrm{Log}(N_{\mu k})$	χ^2/d.f.	χ^2_1/d.f.
1.00–1.05	3.21 ± 0.06	3.42 ± 0.10	1.2 ± 0.3	4.65 ± 0.10	10.4/10	18.7/12
1.05–1.10	3.18 ± 0.08	3.45 ± 0.10	1.1 ± 0.2	4.65 ± 0.10	9.3/10	20.7/12
1.10–1.15	3.18 ± 0.09	3.4 ± 0.2	0.6 ± 0.2	4.75 ± 0.15	6.9/10	9.9/12
1.15–1.20	3.12 ± 0.15	3.4 ± 0.1	1.6 ± 0.5	4.55 ± 0.15	5.9/10	14.0/12

The χ^2/d.f. and χ^2_1/d.f. values are related to the two-slopes and single slope fits respectively.

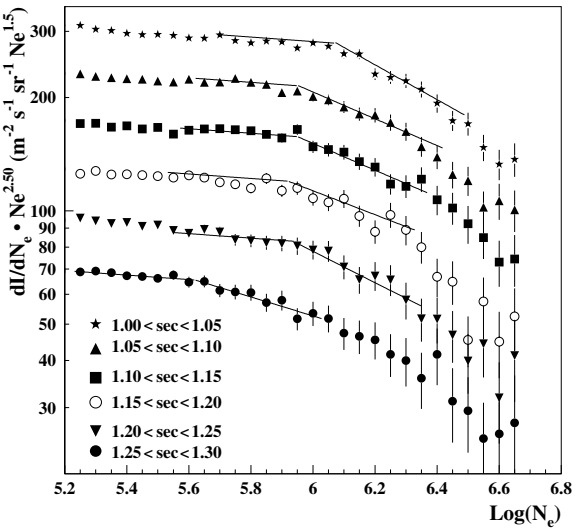

Fig. 3. Differential size spectra measured at different zenith angles (i.e. atmospheric depths). Fits showing the knee position, and its shift with zenith angle are plotted.

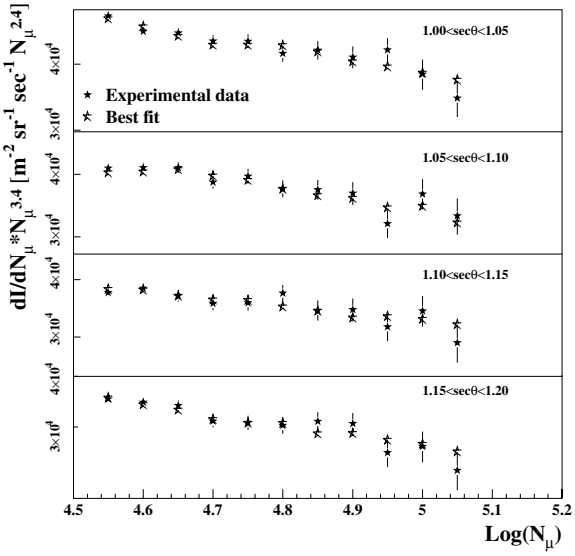

Fig. 4. Differential muon number spectra measured in different intervals of zenith angles (i.e. atmospheric depths), and comparison with the two slopes fits.

components and the different zenith angles is about 35% (i.e. of the order of the experimental uncertainties). This is therefore the level at which the consistency of such intensity measurements can be verified with the present data. The relationship between the spectral indexes $\gamma_e^{1,2}$ and $\gamma_\mu^{1,2}$: $(\gamma_e - 1)(\gamma_\mu - 1) = \alpha \simeq 0.8$ below and above the knee is in general agreement with the value of α expected from the relationship between the e.m. size and the total muon number $N_\mu \propto N_e^\alpha$ (see Section 3.2).

4.2.

The information on the dominating component at the knee, i.e. possibly the bending component, can be obtained from the comparison of the N_e and N_μ size spectra. The consistencies of the spectral slopes and of the intensities at the break make quite reasonable the hypothesis that around the knee we are observing the spectra of the same dominating component. To follow such hypothesis, and improve the consistency tests of the e.m. and muon observations, the experimental spectra have been compared with the simulated ones for single components (p, He, N for CNO, Fe). The comparison is made by constructing for each component a primary energy spectrum fitting the experimental e.m. size spectrum. From such energy spectrum the muon size flux is obtained and is compared to the experimental one. [1] The result is shown in Fig. 5 for vertical events (i.e. with zenith angle of the e.m. shower $\theta \leqslant 17.7°$; since absolute rates are compared, operating at a constant depth is required). The simulated spectra are quite consistent with the experimental data, the agreement being very good for helium primaries. By assuming as systematic uncertainties the differences between the extreme predictions of the interaction models with respect to QGSJET (VENUS and NEXUS, see Fig. 2), we derive the upper and lower limits shown for each primary component in Fig. 5. We obtain that the simulated proton and CNO spectra could hardly be compatible with the experimental one even following the predictions from the extreme existing models included in CORSIKA.

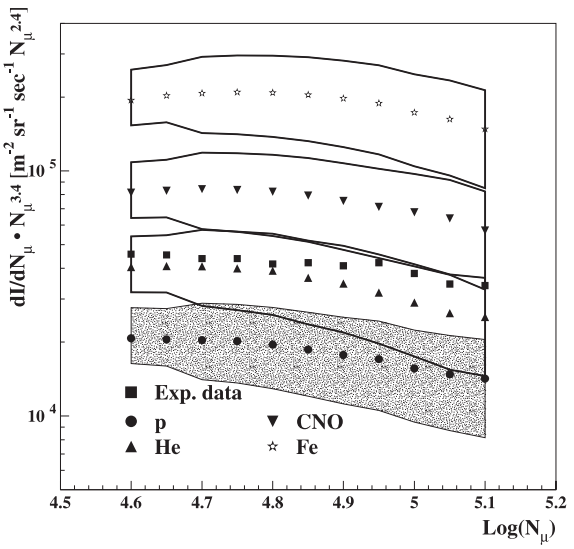

Fig. 5. Experimental muon number spectrum compared with the expectations from individual primaries, whose fluxes $I(E_0)$ reproduce the shower size spectrum in the region of the knee following QGSJET. The bands show the upper and lower limits resulting from the systematic uncertainties in the muon number related to the hadronic interaction model (higher values for VENUS, lower for NEXUS; see text).

5. Analysis of the $\langle \rho_{\mu_{180}} \rangle$ vs (N_e) relationship

As indicator of the EAS muon content, in this analysis, the number of muons recorded by the tracking detector for vertical events ($\theta \leqslant 17.7°$) with core located between 180 and 210 m has been used ($\rho_{\mu_{180}}$ vs N_e) as defined in Section 2). The experimental average values $\langle \rho_{\mu_{180}} \rangle$ are compared with the simulated ones in shower size intervals of amplitude $\Delta \mathrm{Log} N_e = 0.05$.

(i) The experimental data are compared in Fig. 6 with the expectations obtained for single elements from proton up to iron nuclei with the simulation (based on QGSJET) previously described. No one of the single elements reproduces the experimental behavior. At small shower sizes, light elements (in particular He) are very close to the experimental data, while for increasing shower sizes intermediate elements (N and Mg) approach

[1] To compare spectra, large numbers of simulated events are necessary to account for the fluctuations and therefore an hybrid simulation has been developed. Events obtained from the simulations described in Section 3 are binned in energy intervals of amplitude $\Delta \mathrm{Log} E_0 = 0.1$, and inside every bin the distributions of the reconstructed (i.e. including the instrumental and statistical fluctuations, and triggering conditions) e.m. (N_e) and muon (N_μ) sizes have been built. To fit such distributions Log-normal functions have been used. Primary energy spectra have been simulated with different slopes below and above the knee and different knee values, and the related e.m. size spectra have been obtained by sampling the N_e and N_μ values from the quoted Log-normal distributions.

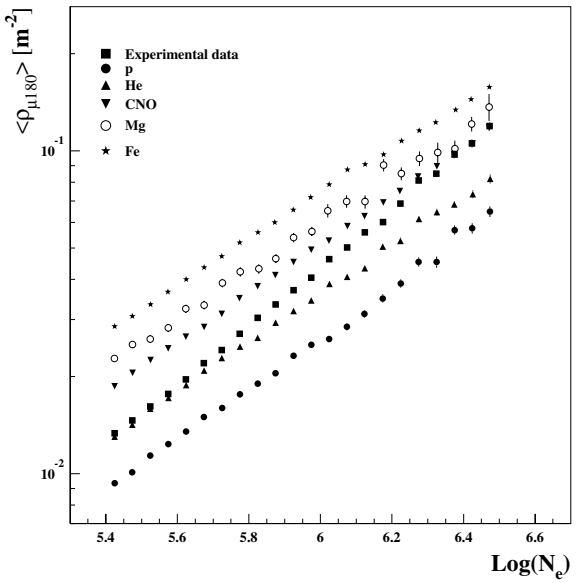

Fig. 6. $\langle \rho_{\mu_{180}} \rangle$ vs N_e: experimental data and expectations from simulations for single elements.

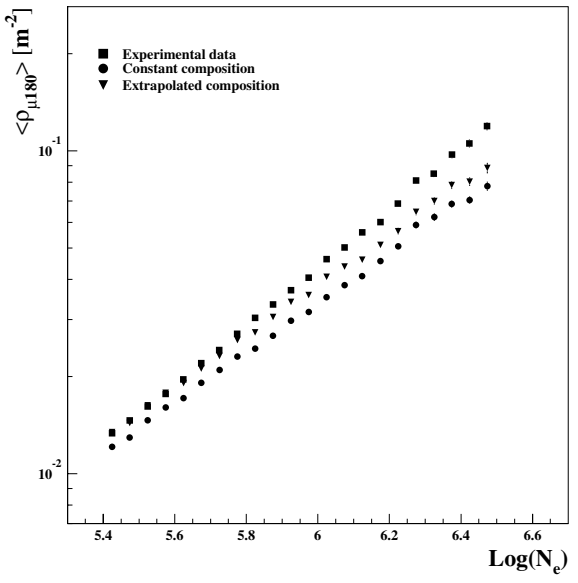

Fig. 7. $\langle \rho_{\mu_{180}} \rangle$ vs N_e: experimental data and comparison with a constant composition and a composition extrapolated from direct measurements (JACEE).

better the data. This is an indication that the average mass $\langle A \rangle$ of the primaries increases with increasing size, and therefore energy, over the whole range.

(ii) An analysis in terms of constant mass composition (namely a composition with constant value of $\langle A \rangle$) has been performed by extrapolating the 1 TeV direct measurements [25] with equal spectral indexes $\gamma = 2.75$ (see Table 3(a)). The $\langle \rho_{\mu_{180}} \rangle$ vs N_e distributions from experimental data and resulting from the simulations based on such primary composition are compared in Fig. 7. For small shower sizes the expectations are close to the experimental points, while with increasing N_e the difference between experimental and simulated values increases, again requiring a composition becoming heavier with increasing primary energy.

(iii) An extrapolated composition as defined in Table 3(b), with the same normalization fluxes at $E_0 = 1$ TeV as the constant one, and different slopes for protons and the heavier components as suggested by JACEE [25] has been built. Such trial composition represents therefore a possible extrapolation of the direct measurements without introducing any change of the spectral indexes at the knee. A slightly better agreement between the simulated and experimental data is obtained below the knee (see Fig. 7), but the slopes of the N_μ–N_e relationship (which reflect the change in composition) are still not conciliable with the experimental

Table 3
Flux values Φ_{TeV} at 1 TeV and spectral indexes adopted for the constant mass composition and the composition extrapolated from the direct measurements

	p	He	N	Mg	Fe
$\Phi_{TeV}(m^{-2}s^{-1}TeV^{-1})$	0.10	0.070	0.032	0.016	0.022
(a) Constant mass composition					
γ	2.75	2.75	2.75	2.75	2.75
(b) Extrapolated composition					
γ	2.79	2.65	2.65	2.65	2.65

ones both below and above the knee, showing that the change in composition observed at lower energies cannot explain the evolution of the primary composition over the whole energy range. Indeed the measured slopes (as defined in Section 3.2) below and above the knee are respectively $\alpha_1^m = 0.890 \pm 0.007$ and $\alpha_2^m = 0.93 \pm 0.02$ (still compatible with a single one: $\alpha^m = 0.907 \pm 0.004$), while the predicted ones for the "extrapolated" composition are: $\alpha_1^e = 0.798 \pm 0.009$ and $\alpha_2^e = 0.79 \pm 0.02$ (all the χ^2/d.f. values of the fits are between 1.1 and 1.4).

(iv) Such results depend of course on the interaction model used (QGSJET), and in some way demonstrate its capability in reproducing the electron and muon numbers at the lowest energies where the extrapolation of the direct measurements is more reliable. To account for the influence of the chosen interaction model, in Section 3.2 the values of α obtained over the whole energy region for the most up to date models included in CORSIKA have been reported. The maximum value is obtained for VENUS ($\alpha_{\mathrm{VENUS}} = 0.820 \pm 0.007$), and is clearly incompatible while the experimental one ($\alpha_{\mathrm{exp}} = 0.907 \pm 0.004$). This shows that no one of the available hadronic interaction models can exclude the increasing average primary mass in the investigated energy range (this is visually shown in Fig. 2).

6. Analysis of the distributions of $N_{\mu_{180}}$ in intervals of N_e

The evolution of the abundances of the primary components vs N_e has been studied by fitting the whole experimental distributions of the detected muon numbers $N_{\mu_{180}}$. Events are selected in the interval of distances 180 m $< r <$ 210 m between the core and the center of the tracker in ranges of shower sizes $\Delta \mathrm{Log}N_e = 0.2$ from $\mathrm{Log}N_e = 5.2$ up to $\mathrm{Log}N_e = 6.6$. The intrinsic resolution of the measurement [2] allows fits with three mass groups: *light*, *intermediate* and *heavy* [26]. The three mass groups are represented respectively through p, N and Fe primaries. In order to evaluate the influence of the choice of the mass groups components on the final result, and the systematic effects due to such choice, a second analysis has been performed, in which the *light* mass group is represented through a mixture of 50% proton and 50% helium, while the *intermediate* and the *heavy* ones are still represented by nitrogen and iron (the two analysis will be denoted respectively as 'p' and 'p + He' in the plots).

The theoretical distributions $f_j(i)$ for each mass group j in the ith bin of $N_{\mu_{180}}$ ($i = 1, M$) in every interval of N_e (used in expression (4)) are obtained from the simulations discussed in Section 3, in which, to account for the real fluctuations, the exponents of the primary spectra (γ) are as near as possible to the real ones (see Table 3 (b)). Since the analysis is performed independently in the different size bins, the chosen value of γ affects the energy distributions only inside the bin itself (i.e. differences Δ_γ of 0.5 affect the mean value of the energy in the bin by less than 10%). The relative abundances of the three mass groups in each bin of N_e are thus obtained directly from the fit of the experimental $N_{\mu_{180}}$ distribution.

The expression minimized to perform such fit is: [3]

$$\chi^2 = \sum_{i=1}^{M} \frac{[f^{\mathrm{d}}(i) - f^{\mathrm{s}}(i)]^2}{\sigma(i)^2} \tag{4}$$

where $f^{\mathrm{d}}(i)$ is the experimental fraction of events of the distribution falling in channel i, and:

$$f^{\mathrm{s}}(i) = \alpha_{\mathrm{L}} f_{\mathrm{L}}(i) + \alpha_{\mathrm{I}} f_{\mathrm{I}}(i) + \alpha_{\mathrm{H}} f_{\mathrm{H}}(i) \tag{5}$$

is the theoretical expression in which α_{L}, α_{I} and α_{H} are the fit parameters representing the relative abundances of the *light*, *intermediate* and *heavy* mass groups. M is the number of channels of the distribution histogram (and is related to the number of d.f.: d.f. $= M - 3$) and $\sigma(i)$ is the error

[2] E.g. in the size range $5.8 < \mathrm{Log}N_e < 6.0$ (as shown in Fig. 8) the average muon number is 3.6 ± 2.1 for protons (it would be 4.2 ± 2.3 for p + He), 6.5 ± 2.7 for CNO, 9.1 ± 3.2 for Fe primaries, where the error indicates the s.d. of the distributions.

[3] Such expression is close to that of a χ^2, although, in principle, it follows a different statistics; in the following we shall refer to it as if it were a genuine χ^2.

on the theoretical expression (5), including the statistical uncertainties of the simulation.

As examples of the results obtained with this procedure, in Figs. 8 and 9 the $N_{\mu_{180}}$ distributions in the size intervals $5.8 < \mathrm{Log}N_e < 6.0$, i.e. just below the knee, arid $6.2 < \mathrm{Log}N_e < 6.4$, i.e. just above it, are reported. In both cases the simulated distributions obtained through the fits approach very well the experimental ones. In the same plots the contributions of each mass group are shown (the 'p' case is given).

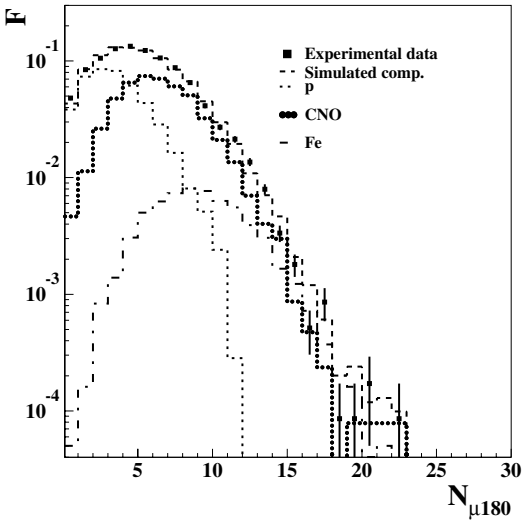

Fig. 8. Comparison between the experimental $N_{\mu_{180}}$ distribution and the fit obtained by means of the three mass groups composition in the range $5.8 < \mathrm{Log}N_e < 6.0$. The contribution of each mass group is also plotted.

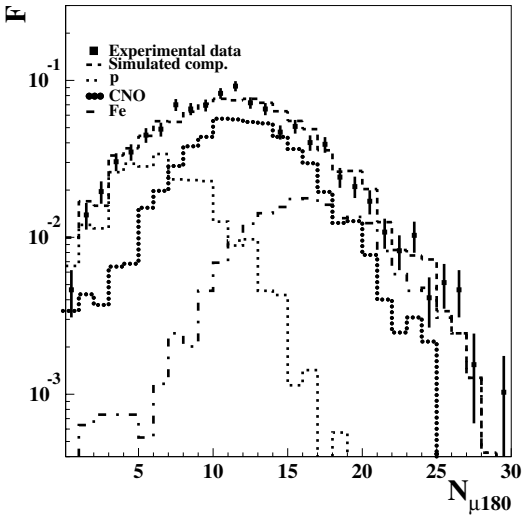

Fig. 9. Same as Fig. 8 in the size range $6.2 < \mathrm{Log}N_e < 6.4$.

The results of the analysis are summarized in Table 4, and the relative abundances of the three components in the seven size intervals are plotted in Fig. 10. In Table 4, beside the χ^2 value describing the goodness of the fit, a second χ^2 value is given (χ^2_1), calculated with the abundances obtained from the fit in the first size bin ($5.2 < \mathrm{Log}N_e < 5.4$). Such χ^2_1 values clearly demonstrate the inconsistency of such composition to represent the data at larger shower sizes. The decreasing weight of the *light* elements and the corresponding increase of the *intermediate* and *heavy* ones is observed in both analysis ('p' and 'p + He'), and thus does not depend on the fraction of protons and helium used to describe the *light* mass group. To account for such uncertainty, and the experimental impossibility of resolving p and He primaries, we will keep the results of both analysis. The χ^2 values reported in Table 4 suggest, anyway, that a fraction of protons in the range below the knee is required, to account for the events characterized by small muon numbers.

The size spectrum corresponding to each mass group is obtained from such relative abundances, using as normalization the experimental size spectrum. The primary energy distributions (see Fig. 11) of each mass group are obtained by selecting from the whole simulated data the events contributing to such size spectra. The corresponding differential energy spectra are plotted in Fig. 12 together with the extrapolations from the direct measurements [25]. At $E_0 \sim 10^6$ GeV the present fluxes and the extrapolated data are in very reasonable agreement, inside the mass groups approximation.

The reconstructed spectrum of the *light* mass group results steeper ($\gamma_{\mathrm{p,He}} > 3.1$) than the one obtained from the direct measurements. A break in the CNO spectrum is possibly observed ($\gamma_{\mathrm{CNO},1} \simeq 2.5$, $\gamma_{\mathrm{CNO},2} \simeq 3.3$) at primary energy $E_k^{\mathrm{CNO}} \simeq (6\text{–}7) \times 10^6$ GeV. Inside the uncertainties of the assumptions for the light component ('p' or 'p + He') a unique spectral index ($\gamma_{\mathrm{CNO}} \simeq 2.75$)

Table 4
Relative abundances of the three components in seven intervals of N_e obtained by fitting the $N_{\mu 180}$ distributions, and χ^2 values of the fits (some large χ^2 values are due to the mass group approximation, and the nonseparable contributions of protons and helium)

LogN_e	5.2–5.4	5.4–5.6	5.6–5.8	5.8–6.0	6.0–6.2	6.2–6.4	6.4–6.6
α_p	0.62 ± 0.01	0.62 ± 0.02	0.56 ± 0.02	0.44 ± 0.02	0.34 ± 0.02	0.26 ± 0.03	0.18 ± 0.04
α_N	0.34 ± 0.02	0.33 ± 0.03	0.37 ± 0.02	0.49 ± 0.02	0.60 ± 0.04	0.56 ± 0.05	0.65 ± 0.07
α_{Fe}	0.04 ± 0.01	0.05 ± 0.01	0.07 ± 0.01	0.06 ± 0.01	0.07 ± 0.02	0.19 ± 0.02	0.23 ± 0.04
χ^2/d.f.	17/11	53/14	42/18	25/21	36/25	35/29	42/36
χ^2_1/d.f.	17/14	56/17	129/21	279/24	347/28	489/31	340/39
$\alpha_p + He$	0.83 ± 0.03	0.84 ± 0.05	0.76 ± 0.04	0.60 ± 0.03	0.46 ± 0.02	0.37 ± 0.03	0.24 ± 0.05
α_N	0.10 ± 0.04	0.06 ± 0.07	0.14 ± 0.06	0.30 ± 0.04	0.45 ± 0.03	0.43 ± 0.05	0.55 ± 0.08
α_{Fe}	0.08 ± 0.02	0.11 ± 0.03	0.10 ± 0.02	0.10 ± 0.02	0.09 ± 0.01	0.21 ± 0.03	0.26 ± 0.04
χ^2/d.f.	61/11	122/14	127/18	54/21	20/25	33/29	42/36
χ^2_1/d.f.	61/14	135/17	192/21	321/24	391/28	456/31	357/39
N	258,384	120,668	54,492	23,356	10,106	3890	1328

The χ^2_1 values are equivalent to the χ^2 ones, but obtained in each size interval by using the composition of the lower size bin. N is the number of experimental events used in each interval. The two cases, in which the light mass group is represented by "p" and "50% p + 50% He", are given.

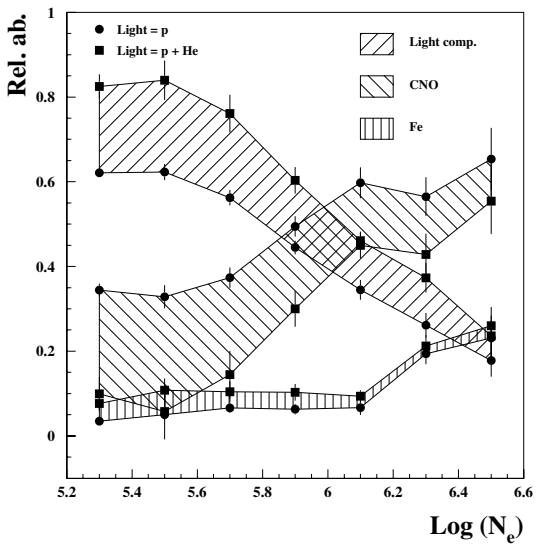

Fig. 10. Relative abundances of the three mass groups in different intervals of shower sizes.

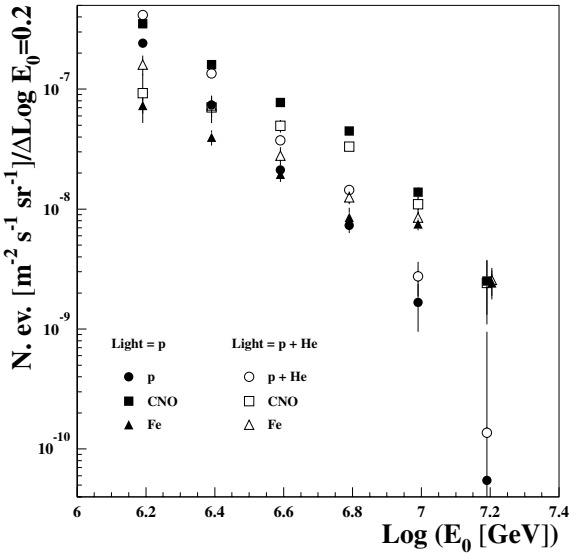

Fig. 11. Distributions of the number of events of each mass group in energy intervals $\Delta \mathrm{Log}E_0 = 0.2$.

could also be compatible with the data. No steepening is observed in the spectrum of the heavier mass group (iron): the index of the power law spectrum $\gamma_{Fe} \simeq 2.3$–2.7 fits the data over the whole energy range and is compatible with the one measured in the TeV range by the direct experiments.

The relative abundances: $\alpha_L^{E_0}, \alpha_I^{E_0}, \alpha_H^{E_0}$, and the evolution of $\langle \ln A \rangle$ vs primary energy extracted from the data of Fig. 11 are shown in Figs. 13 and

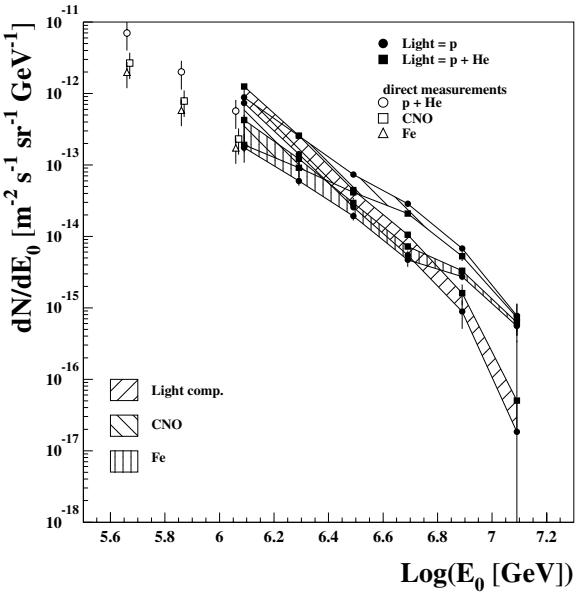

Fig. 12. Energy spectra of the three mass groups. To be consistent with the present analysis, in the direct measurements (reported for comparison) the light mass group includes proton and helium primaries.

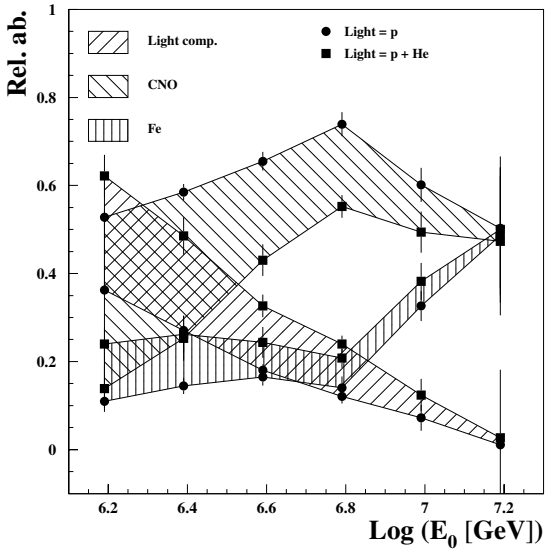

Fig. 13. Relative abundances of the three mass groups in different intervals of primary energies.

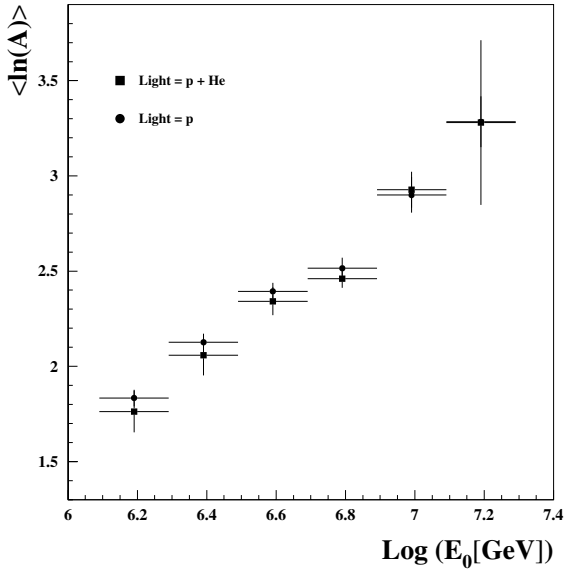

Fig. 14. Average value of $\ln(A)$ vs primary energy E_0.

14. The increasing value of $\langle \ln A \rangle$ and the changes in spectral slopes occurring at lower energies for lighter primaries is in accord with the data presented by the KASCADE Collaboration [8,27]. The agreement concerning the $\langle \ln A \rangle$ behavior is also quite good when comparing with the CAS-

AMIA [28] and the combined EAS-TOP and MACRO [21] measurements in which the analysis are performed in terms of a two mass groups (*light*, *heavy*) primary beam. Particularly significant is the comparison with the EAS-TOP and MACRO data, due to the much higher muon energies recorded in such experiment, showing that the obtained composition does not depend on the rapidity region of production of the secondaries.

7. Conclusions

The study of the cosmic ray composition around the knee of the primary spectrum has been carried out through the analysis of the e.m. and muon ($E_\mu^{\rm th} \approx 1$ GeV) Extensive Air Shower components recorded at EAS-TOP (2005 m a.s.l, National Gran Sasso Laboratories). The data are analyzed by means of comparisons with simulations performed in the frame of CORSIKA/QGSJET.

The experimental N_e and N_μ spectra in the region of the knee are consistent and well reproduced by the simulation. This suggests that the same primary component dominates both spectra in such region, and is in very good agreement with the expectations from helium primaries. This is in accord with the extrapolation of the direct JACEE measurements [25] and the combined EAS-TOP Cherenkov light and MACRO data [19]. Proton and CNO primaries are hardly compatible with the experimental data, even assuming the maximum systematic uncertainties on the muon yield (corresponding to the maximum differences in the predictions between the up to date models that have been tested). If therefore helium primaries are responsible of the main observed knee, the corresponding bending energy for their spectrum is $E_k^{He} \approx (3.5 \pm 0.3) \times 10^6$ GeV.

Both the mean values and the full distributions of the muon numbers recorded as a function of shower size have been studied. From the analysis of the mean values a good agreement is found with the simulated data obtained following the extrapolations of the direct measurements as reported by JACEE below the knee. This proves a "phenomenological" reliability of the hadron interaction model (CORSIKA-QGSJET) used in the analysis. To account for the slope of the $N_\mu - N_e$ relationship, an increasing average primary mass is required over the whole range. No one of the most up to date models included in CORSIKA provides a value of such dependence compatible with the measured one. Therefore no one of them can exclude the increasing average primary mass in the investigated energy range. The differences introduced by the choice of a specific interaction model are therefore of minor significance with respect to such conclusion.

The full distributions of the recorded muon numbers at 180 m – 210 m from the core, $N_{\mu_{180}}$, in fixed intervals of shower size, are well reproduced by means of three mass groups primaries (*light*, *intermediate* and *heavy*, represented respectively by protons or '50% protons + 50% helium', nitrogen and iron).

The obtained evolutions of their spectra through the knee region lead to:

(a) a steep spectrum of the *light* mass group ($\gamma_{\rm p,He} > 3.1$);
(b) a possible change in slope of the *intermediate* one at $E_k^{\rm CNO} \approx (6\text{–}7) \times 10^6$ GeV or a spectrum, on the average, harder than for the *light* mass group ($\gamma_{\rm CNO} \simeq 2.75$);
(c) a constant slope for the spectrum of the *heavy* primaries ($\gamma_{\rm Fe} \simeq 2.3\text{–}2.7$), consistent with the direct measurements.

Such features do not depend on the relative weights of the proton and helium components used to construct the *light* mass group.

The increasing average logarithmic mass ($\langle \ln A \rangle$) in one decade of primary energy (1.5×10^6–1.5×10^7 GeV), amounts to A $\Delta\langle \ln A \rangle = 1.5 \pm 0.5$, corresponding to a rather fast leakage of the *light* mass group.

The result is in good agreement with the one obtained from the analysis of the combined EAS-TOP (N_e) and MACRO (N_μ) data, in which the detected muons ($E_\mu > 1.3$ TeV) are produced in a different rapidity range (i.e. above the central region) [21]. This demonstrates the compatibility of the predictions of QGSJET with the experimental data in describing the hadron interactions over a wide energy range of the secondaries.

The observed evolution of the composition and the different spectra of the primary mass groups, also when compared to the direct data, are therefore in general agreement with the expectations from the standard acceleration and propagation models of cosmic ray primaries in our Galaxy, predicting rigidity dependent breaks in the spectra of the different primaries.

Acknowledgements

The continuous cooperation of the National Gran Sasso Laboratories, as well as of Mr. C. Barattia, R. Bertoni, G. Giuliani, A. Giuliano, and G. Pirali are gratefully acknowledged.

References

[1] G.V. Kulikov, G.B. Khristiansen, Sov. Phys. JEPT 35 (1958) 441.
[2] M. Nagano et al., J. Phys. G 10 (1984) 1295.
[3] B. Peters, in: Proceedings of the 6th ICRC, vol. 3, 1960, p. 157.
[4] G.T. Zatsepin et al., Izv. Akad. Nauk USSR S.P. 26 (1962) 685.
[5] A.M. Hillas, in: Proceedings of the 16th ICRC, vol. 8, 1979, p. 7.
[6] A.D. Erlykin, A.W. Wolfendale, J. Phys. B 23 (1997) 979.
[7] M. Aglietta et al. (EAS-TOP Coll.), Nucl. Phys. B 85 (2000) 318.
[8] T. Antoni et al. (KASCADE Coll.), Astrop. Phys. 16 (2002) 373.
[9] O.A. Gress et al. (Tunka Coll.), in: Proceedings of the 25th ICRC, vol. 4, 1997, p. 129.
[10] J.R. Hörandel et al. (KASCADE Coll.), in: Proceedings of the 26th ICRC, vol. 1, 1999, p. 337.
[11] M. Aglietta et al. (EAS-TOP Coll.), Astrop. Phys. 10 (1999) 1.
[12] N.N. Kalmykov et al., Nucl. Phys. B 52 (1997) 17.
[13] D. Heck, J. Knapp, Extensive Air Shower simulation with CORSIKA (5.61), Forschungszentrum Karlsruhe Report FZKA 6019, 1998.
[14] M. Aglietta et al. (EAS-TOP Coll.), Nucl. Instr. and Meth. A 336 (1993) 310.
[15] K. Karnata et al., Suppl. Prog. Theo. Phys. 6 (1958) 93.
[16] R. Adinolfi Falcone et al. (EAS-TOP Coll.), Nucl. Instr. and Meth. A 420 (1999) 117.
[17] Application Software Group and Network Division, GEANT: Detector Description and Simulation Tool 3.21, CERN W5013, 1994.
[18] M. Aglietta et al. (EAS-TOP Coll.), Astrop. Phys. 19 (2003) 329.
[19] M. Bertaina et al. (EAS-TOP and MACRO Coll.), in: Proceedings of the 27th ICRC, vol. 1, 2001, p. 14;
M. Aglietta et al. (EAS-TOP and MACRO Coll.), Astropart. Phys. 21 (2004) 223.
[20] T. Antoni et al. (KASCADE Coll.), Nucl. Part. Phys. 27 (2001) 1785.
[21] G. Navarra, et al., (EAS-TOP and MACRO Coll.), in: Proceedings of the 27th ICR21C, vol. 1, 2001, p. 120;
M. Aglietta et al. (EAS-TOP and MACRO Coll.), Astrop. Phys. 20 (2004) 641.
[22] H.J. Drescher et al., Phys. Rep. 350 (2001) 93.
[23] J. Ranft, Phys. Rev. D 51 (1995) 64, hep-ph/9911232 (1999).
[24] K. Werner, Phys. Rep. 232 (1993) 87.
[25] Y. Takahashi et al. (JACEE Coll.), Nucl. Phys. B 60 (1998) 83.
[26] B. Alessandro et al. (EAS-TOP Coll.), in: Proceedings of the 27th ICRC, vol. 1, 2001, p. 124.
[27] K.-H. Kampert et al. (KASCADE Coll.), in: 27th ICRC, Invited, Rapporteur and Highlight Papers, 2001, p. 240.
[28] M.A.K. Glasmacher et al. (CASA-MIA Coll.), Astrop. Phys. 12 (1999) 1.